Trading Electrons: Predicting DART Spread Spikes in ISO Electricity Markets

Emma Hubert[*]   Dimitrios Lolas[†]   Ronnie Sircar[†]

January 7, 2026

Abstract

We study the problem of forecasting and optimally trading day-ahead versus real-time (DART) price spreads in U.S. wholesale electricity markets. Building on the framework of [9], we extend spike prediction from a single zone to a multi-zone setting and treat both positive and negative DART spikes within a unified statistical model. To translate directional signals into economically meaningful positions, we develop a structural and market-consistent price impact model based on day-ahead bid stacks. This yields closed-form expressions for the optimal vector of zonal INC/DEC quantities, capturing asymmetric buy/sell impacts and cross-zone congestion effects. When applied to NYISO, the resulting impact-aware strategy significantly improves the risk–return profile relative to unit-size trading and highlights substantial heterogeneity across markets and seasons.

1   Introduction

In U.S. wholesale electricity markets operated by Independent System Operators and Regional Transmission Organizations (ISOs/RTOs), trading is organized as a two-settlement system: a Day-Ahead Market (DAM), in which schedules and prices for the following operating day are determined, and a Real-Time Market (RTM), in which actual imbalances are settled at higher frequency. The difference between these two prices—the day-ahead real-time spread (DART)—is a central risk factor for both financial and physical market participants and can be interpreted as a market-implied forecast error up to an embedded risk premium [19]. Large deviations often arise from transmission congestion, load forecast errors, unit commitment constraints, and network contingencies, and they can generate substantial profit opportunities for traders capable of anticipating extreme DART events. Empirical works document that such extreme price movements are short-lived, clustered, and closely linked to binding network constraints and unexpected demand shocks [17, 4, 21, 23].

In NYISO (New York ISO) and ISO–NE (ISO New England), market participants may take purely financial day-ahead positions through virtual bidding. An INC trade (virtual

---

[*]CEREMADE, Université Paris Dauphine & PSL Research University.
[†]Department of Operations Research & Financial Engineering, Princeton University.

demand) of size $q > 0$ buys energy in the Day-Ahead Market at unit price P^{DA} and sells it back in the Real-Time Market at price P^{RT}, yielding a payoff $(P^{\mathrm{RT}} - P^{\mathrm{DA}}) \times q$, while a DEC trade (virtual supply) does the opposite, yielding $(P^{\mathrm{DA}} - P^{\mathrm{RT}}) \times q$. Thus, the problem faced by a virtual market participant is simultaneously predictive and operational:

1. reliably forecast where and when large DART spreads will occur, and
2. translate these forecasts into profitable day-ahead positions under realistic market impact.

A growing literature studies DART spreads and virtual bidding from both predictive and structural perspectives, emphasizing the role of congestion, risk premia, and limits to arbitrage in two-settlement electricity markets [19]. Early empirical work documents the prevalence and economic drivers of DART price deviations and the role of congestion and forecast errors in shaping these spreads [3]. Subsequent studies examine the profitability and limits of virtual bidding strategies, emphasizing the importance of transaction costs, market power, and convergence effects. More recently, machine-learning approaches have been applied to electricity price and DART forecasting, showing that extreme price dislocations can be predicted with economically meaningful accuracy [16, 9, 24, 8]. From a structural perspective, electricity prices are often modeled as arising from the intersection of aggregate supply and demand curves, with local properties of the bid stack governing price sensitivity to quantity shocks [5]. Related structural approaches that jointly model load and price dynamics for risk management and hedging in electricity markets include [6].

The recent study [9] provides a predictive framework for identifying and trading extreme DART spikes in Long Island, the second largest zone in NYISO. Their results demonstrate that spike forecasting is feasible and economically valuable. However, their study has two main limitations: (i) trades are sized using a fixed quantity rather than an optimized portfolio of zonal exposures, and (ii) the strategy is evaluated only on a single zone. Here, we address the central operational question faced by large traders: how to scale multi-zone virtual positions when submitting thousands of MWh into the Day-Ahead Market without eroding profits through market impact.

Contributions. This paper extends the framework of [9] in four key directions:

1. **Multi-zone, two-sided DART spike forecasting.** We jointly model extreme positive and negative DART spreads across all NYISO zones, allowing for correlated bidirectional spike dynamics across locations.

2. **A structural, economically consistent model of market impact.** Using day-ahead bid stacks, we estimate both system-wide energy impact coefficients—capturing how net long or short virtual load shifts the DA clearing price—and zone-specific congestion sensitivities. This yields a linear–quadratic impact model linking trade size to expected price perturbation.

3. **Optimal scaling of virtual positions.** We derive closed-form expressions for the profit-maximizing vector of zonal quantities, incorporating asymmetric buy/sell impacts and cross-zone interactions. This allows us to determine how large a trade should be in each zone, not merely whether a trade should be executed.

4. **Empirical validation at scale.** When deployed on 2022–2025 out-of-sample data in multiple zones of three ISO regions—NYISO, ISO–NE and ERCOT[1]—the resulting strategy achieves substantial profitability and remains robust across market regimes, including the extreme temperatures observed during Summer 2025.

Model overview. Our methodology proceeds in three stages. First, we train in Section 3 zone-level classifiers to forecast extreme positive and negative DART events using historical load, price, and congestion features described in Section 2. Second, conditional on a directional signal, we estimate the expected DART spread and the local price impact implied by the observed day-ahead bid stack (Section 4.3). Finally, we solve a quadratic optimization problem that jointly determines the optimal vector of zonal virtual positions, explicitly accounting for asymmetric system-wide and local market impact (Section 4.2). This separation between signal generation and impact-aware sizing allows predictive accuracy and economic consistency to be evaluated independently.

Overall, our results show that DART forecasting and virtual bidding must be treated as a joint problem: forecasts alone are insufficient unless paired with a principled model of price impact and a rigorous scaling rule. By combining predictive modeling, structural analysis of bid stacks, and multi-zone optimization, this paper provides a comprehensive framework for scalable and economically consistent virtual trading in U.S. wholesale electricity markets.

2 Predictive Framework and Statistical Model

This section develops a unified framework for forecasting day-ahead versus real-time (DART) price spreads in U.S. wholesale electricity markets, with an empirical focus on NYISO, ISO–NE, and ERCOT. Figure 1 shows the zonal layouts for the three regions.
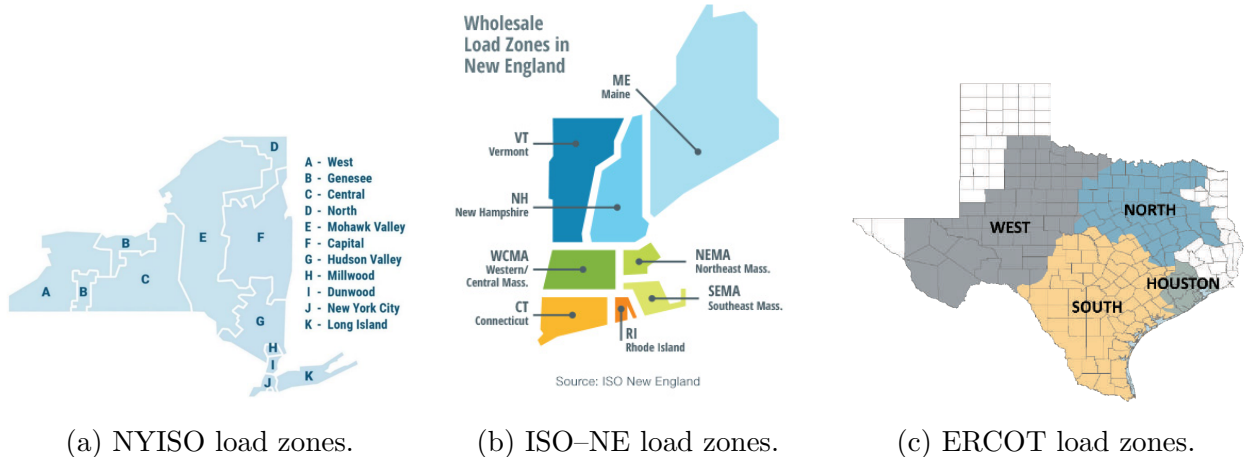

(a) NYISO load zones. (b) ISO–NE load zones. (c) ERCOT load zones.

Figure 1: Zonal maps for NYISO, ISO–NE, and ERCOT.

---

[1]ERCOT does not permit virtual trading, but physical resources face analogous DART exposure when deciding whether to self-commit in the DAM.

2.1 Data Construction

For each of the three markets, we construct an hourly panel containing day-ahead and real-time prices, system and zonal load forecasts, and a set of exogenous covariates. These include lagged DART values (24h/48h), lagged load forecast errors, hour-of-day and month-of-year indicators, holiday/weekend dummies, and seasonal effects. In practice, all features are constructed using a common set of definitions, lag structures, and calendar conventions across the markets, enabling direct comparability. All market data were obtained from the public data portals of the corresponding system operators, namely ERCOT [7], ISO New England [13], and NYISO [20]. Data access and aggregation were facilitated using the GridStatus platform (https://www.gridstatus.io).

2.2 Feature Labeling

As day-ahead bids must be submitted well in advance of the operating day, all predictors are constructed using only data available strictly before the corresponding Day-Ahead Market's gate-closure time:

$$\text{NYISO: 05:00,} \qquad \text{ISO–NE: 10:30,} \qquad \text{ERCOT: 10:00.}$$

This implies a prediction horizon between 19 and 43 hours, depending on the market, and ensures that the forecasting exercise is entirely free of look-ahead bias.

Thus, the feature vector $X_{t,z,m} \in \mathbb{R}^d$ available at the day-ahead decision time for the operating hour t, in zone z of market m, is constructed using only information available prior to the Day-Ahead Market close and consists of: (i) lagged DART values at 24h and 48h horizons; (ii) zonal and system-level day-ahead load forecasts; (iii) lagged zonal and system-level load forecast errors; (iv) calendar indicators for hour-of-day, month-of-year, and holidays/weekends; and (v) season-of-year indicators (Winter, Summer, Shoulder).

The dimension d corresponds to the total number of covariates after feature construction, including calendar effects, lagged price and load variables, system-level aggregates, and zone fixed effects. The exact value of d thus depends on the market and feature availability. For example, in the NYISO application considered below, this results in a feature dimension of $d = 50$, which is significantly larger than $d = 9$ used in [9]. Specifically, each hourly observation is represented by a 50-dimensional feature vector X_t. This vector concatenates four zone-level predictors—day-ahead load forecasts, lagged DART values (24h and 48h), and lagged load forecast errors—for each of the 11 zones ($4 \times 11 = 44$), together with six calendar covariates encoding weekend, holiday, diurnal, and seasonal effects.

2.3 Spike Definition and Logistic Regression Models

Given the DART value at time t, in zone z of market m, we define binary labels for negative and positive DART spikes as

$$y_{t,z,m}^{\text{neg}} = \mathbf{1}_{\{\text{DART}_{t,z,m} \leq -\gamma_{\text{neg}}(m)\}}, \qquad y_{t,z,m}^{\text{pos}} = \mathbf{1}_{\{\text{DART}_{t,z,m} \geq \gamma_{\text{pos}}(m)\}},$$

where the market-specific thresholds $\gamma_{\text{neg}}(m)$ and $\gamma_{\text{pos}}(m)$ are calibrated through exploratory analysis and validation. These labels isolate the economically meaningful extremes of the

DART distribution that are most relevant for virtual trading strategies. Our first objective is to perform a logistic regression to predict DART spikes.

For each zone z of market m and spike type, we define the predicted spike probability at time t as

$$p_{t,z,m} = \mathbb{P}(y_{t,z,m} = 1 \mid X_{t,z,m}) = \sigma(\beta_{z,m}^{\top} X_{t,z,m}), \quad \text{with} \quad \sigma(u) = \frac{1}{1 + e^{-u}}. \tag{1}$$

The coefficients $\beta_{z,m}$ are obtained by minimizing the following cross-entropy loss for each zone z:

$$\min_{\beta} \sum_{t} \left[y_{t,z,m} \left(-\log p_{t,z,m} \right) + (1 - y_{t,z,m}) \left(-\log(1 - p_{t,z,m}) \right) \right].$$

Training windows differ across markets due to data availability (NYISO: 2015–2019; ISO–NE and ERCOT: 2018–2022), and a separate validation period is used to tune probability thresholds.

Model selection. Before settling on logistic regression, we performed an extensive comparison across several supervised learning methods, including random forests, gradient-boosted trees and feed-forward neural networks [11]. While some nonlinear models achieved marginally higher in-sample classification accuracy, they offered no consistent improvement in out-of-sample trading P&L. This occurs because the spike events of interest are extremely rare and the feature set is largely linear in its predictive structure; consequently, more flexible models exhibit a tendency to overfit the noise in the training data and produce unstable probability forecasts. Logistic regression, by contrast, delivered the most robust and interpretable out-of-sample performance across all three markets, and produced stable probability estimates that translate reliably into trading signals. For these reasons, all subsequent results and scaling analyses are reported using the logistic models.

3 Empirical Performance of Benchmark Strategies

In this section, we study DART spreads and the performance of the benchmark spike-based INC/DEC strategies described below in Section 3.1, across the three major U.S. power markets: NYISO, ISO–NE, and ERCOT. All analyses use hourly data and a common modeling framework, with separate classifiers for positive and negative DART spikes calibrated on a validation set and evaluated out-of-sample.

Pooling information across zones is essential in NYISO, where congestion and losses generate substantial zonal heterogeneity. In contrast, ISO–NE and ERCOT exhibit highly synchronized zonal DART movements, so that a single representative zone captures most of the relevant variation.

3.1 Benchmark INC and DEC Strategies

Recall that $p_{t,z,m}$ denotes the predicted probability of a DART spike at time t in zone z of market m, as defined in (1). In [9], a trade is executed whenever

$$p_{t,z,m} \geq \tau_{z,m},$$

where $\tau_{z,m}$ is a zone-specific threshold. The predictive model used to estimate the probability $p_{t,z,m}$ of a DART spike, conditional on the feature vector $X_{t,z,m}$, is trained on a historical training set, while $\tau_{z,m}$, $\gamma_{\text{neg}}(m)$ and $\gamma_{\text{pos}}(m)$ are selected to maximize P&L on a separate validation set under unit-size trading and no price impact. All performance results reported below are evaluated on a held-out test set.

We study two benchmark strategies:

1. **INC-only**: trade when a negative DART spike is predicted, earning $-\text{DART}_{t,z,m}$;

2. **DEC-only**: trade when a positive DART spike is predicted, earning $+\text{DART}_{t,z,m}$.

These strategies provide a clean baseline for comparing predictive performance across markets and zones. Building on this benchmark framework, we will extend in Section 4.2 the single-zone trading rule to a joint multi-zone optimization problem with endogenous position sizing and price impact.

3.2   P&L in NYISO

For NYISO, we work with hourly data from 2015–2025 across eleven load zones, and focus the discussion on six large-demand zones: CAPITL, CENTRL, LONGIL, NORTH, NYC, and WEST. We adopt the chronological split

$$\text{Train: 2015–2019,} \qquad \text{Validation: 2020–2021,} \qquad \text{Test: 2022–2025.}$$

Separate logistic classifiers are fit for positive and negative DART spikes on the training set, with spike thresholds and probability cutoffs selected on the validation set to maximize unit-size P&L. The resulting thresholds used in the NYISO analysis are

$$\gamma_{\text{pos}} = 5\$/\text{MWh}, \qquad \gamma_{\text{neg}} = 30\$/\text{MWh}.$$

We tune the probability cutoffs τ_{pos} and τ_{neg} separately for each zone. For example, in NYC the selected cutoffs are $(\tau_{\text{pos}}, \tau_{\text{neg}}) = (0.75, 0.9)$, while for Long Island they are $(0.7, 0.9)$.

Figures 2(a)–(d) report cumulative P&L over the 2022–2025 test period for INC-only and DEC-only benchmark strategies in NYC and Long Island, the two zones with the highest demand. Corresponding results for the remaining zones are presented in Figures 8(a)–(h) in the Appendix. The figures highlight pronounced cross-zonal heterogeneity: while some regions exhibit persistent profitability from DEC positions, others display stronger performance for INC trading.

Tables 5 and 6 (in the Appendix) report cumulative P&L by zone, which we relate to the yearly mean DART spreads shown in Table 7. Zones with systematically positive DART averages (e.g., CAPITL or, in earlier years, LONGIL) tend to favour DEC strategies, whereas zones with negative or mixed averages (such as NYC in the post-2022 period) are more aligned with INC trading. This structural bias in the DART distribution helps explain cross-zonal differences in profitability and provides guidance on whether a zone is better approached with INC-only, DEC-only, or mixed strategies.

Cross-zone dependence remains strong throughout NYISO, as shown in Table 8, but varies meaningfully across groups of zones. Upstate zones exhibit particularly high correlations in

(a) NYC — INC

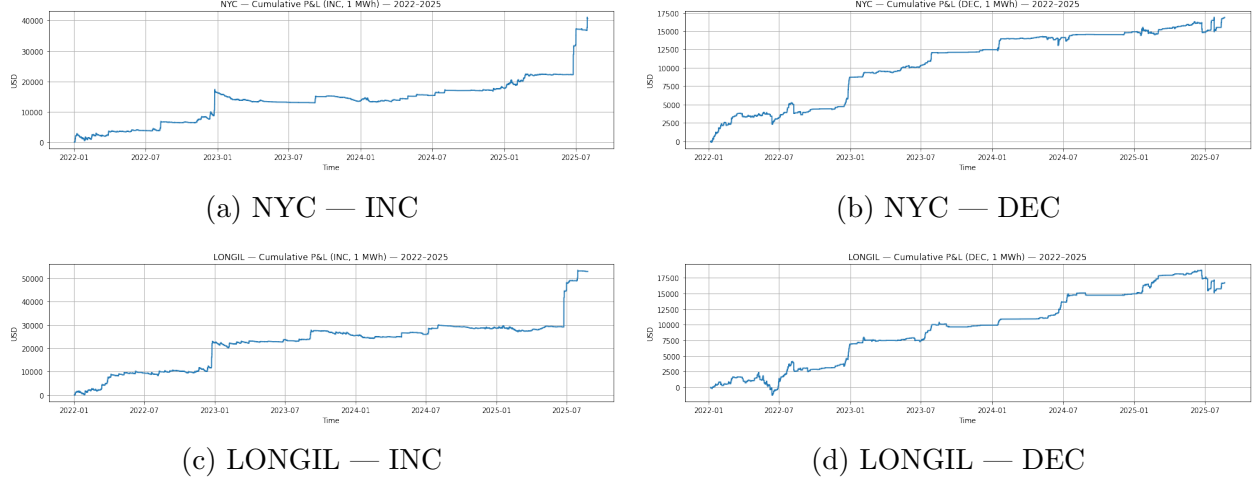(b) NYC — DEC

(c) LONGIL — INC

(d) LONGIL — DEC

Figure 2: NYISO: cumulative P&L for NYC and Long Island under the INC/DEC benchmark strategy.

DART spreads, while downstate zones form a tightly interconnected cluster. This pattern reflects localized congestion and loss effects superimposed on system-wide price movements, and motivates pooling information across zones while retaining zone-specific features in the predictive models.

3.3 P&L in ISO–NE

We perform a parallel analysis on ISO New England, which consists of eight load zones, using hourly data from November 2018 to October 2025. DART spreads across ISO–NE zones are almost perfectly correlated, as we see in Table 9, indicating that economically relevant variation is predominantly system-wide rather than zonal. To avoid redundant signals, we therefore conduct the spike-prediction and trading analysis on a single representative zone, Maine (ME).

Given the shorter sample relative to NYISO, we adopt the split

$$\text{Train: } 2018\text{–}2022, \qquad \text{Validation: } 2023, \qquad \text{Test: } 2024\text{–}2025.$$

Separate classifiers are fit for positive and negative DART spikes, with spike thresholds and probability cutoffs tuned on the validation set. For the Maine load zone in ISO–NE, the resulting parameters are

$$\gamma_{\text{pos}} = 2\$/\text{MWh}, \qquad \gamma_{\text{neg}} = 8\$/\text{MWh}, \qquad \tau_{\text{pos}} = 0.70, \qquad \tau_{\text{neg}} = 0.90.$$

Figure 3 shows the cumulative P&L curves for the INC-only and DEC-only benchmark strategies on the 2024–2025 test period. Overall performance is weaker than in NYISO, with most profits arising from DEC trades, while INC positions are triggered less frequently due to both the smaller negative-spike threshold and the model's lower predictive sharpness in this market.
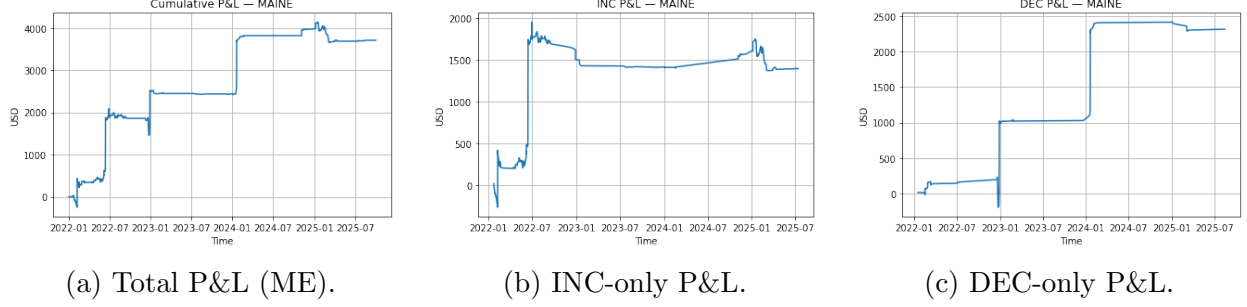
7

(a) Total P&L (ME).   (b) INC-only P&L.   (c) DEC-only P&L.

Figure 3: ISO–NE MAINE zone — P&L curves for overall, INC-only, and DEC-only strategies on the 2024–2025 test period.

3.4 P&L in ERCOT

We next analyze ERCOT using hourly data from 2018–2025 across its four principal load zones: North, South, West, and Houston. DART spreads across ERCOT zones are extremely highly correlated (Table 10), with pairwise correlations exceeding 0.97, indicating that DA–RT dynamics are effectively system-wide. As a result, all zones generate nearly identical predictions and trading behavior; we therefore focus on the WEST zone for concreteness.

Given the shorter sample relative to NYISO, we adopt the split

$$\text{Train: 2018–2022}, \qquad \text{Validation: 2023}, \qquad \text{Test: 2024–2025}.$$

Spike thresholds and probability cutoffs are tuned on the validation set. For WEST, the resulting parameters are

$$\gamma_{\text{pos}} = 15\$/\text{MWh}, \qquad \gamma_{\text{neg}} = 10\$/\text{MWh}, \qquad \tau_{\text{pos}} = 0.75, \qquad \tau_{\text{neg}} = 0.90.$$

Figure 4 reports the total, INC-only, and DEC-only benchmark strategy P&L curves on the 2024–2025 test period. Most profits arise from the DEC side, while INC trades perform well initially but give back a large fraction of early gains.
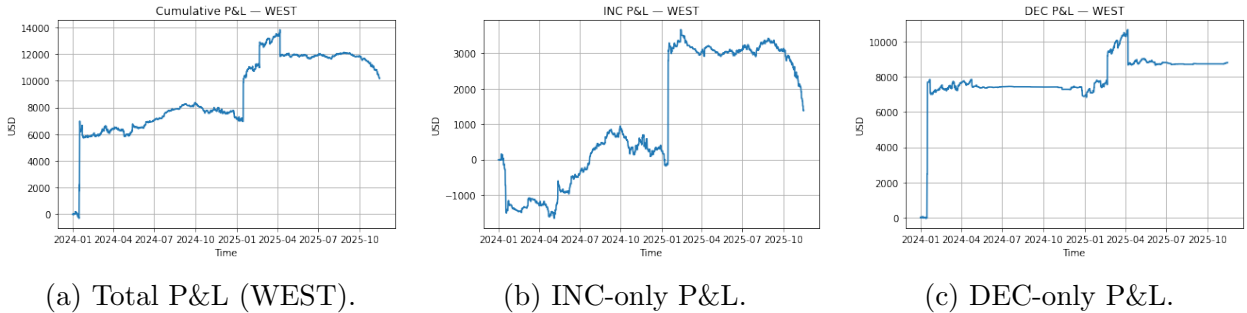

(a) Total P&L (WEST).   (b) INC-only P&L.   (c) DEC-only P&L.

Figure 4: ERCOT WEST zone — P&L curves for overall, INC-only, and DEC-only strategies on the 2024–2025 test period.

3.5 Cross–Market Comparison

Tables 8, 9, and 10 highlight pronounced differences in cross-zonal DART dependence across markets. In ERCOT and ISO–NE, DART spreads are almost perfectly synchronized across zones, indicating that DA–RT deviations are driven primarily by system-wide factors. Consequently, zone-level behaviour in these markets is largely redundant, and a single representative zone captures most relevant variation. By contrast, NYISO exhibits substantially weaker and more heterogeneous cross-zonal correlations, reflecting localized congestion, losses, and transmission constraints. This structural heterogeneity implies that DART dynamics in NYISO cannot be reduced to a single system factor, making multi-zone modelling essential.

To provide distributional context for the spike thresholds and trading activity across markets, Table 11 reports empirical DART quantiles on the training samples for representative zones: NYISO LONGIL, ISO–NE ME, and ERCOT WEST. NYISO exhibits heavier intermediate and upper tails, with substantially larger 90th–99th percentiles relative to ISO–NE and ERCOT.

Taken together, the heavier-tailed DART distribution in NYISO helps explain its greater trading profitability relative to ISO–NE and ERCOT: larger and more frequent spikes generate a richer set of economically meaningful opportunities, on which predictive signals can be exploited more often. Differences in observed INC and DEC activity across markets therefore reflect both underlying market structure and the predictive sharpness of the model, rather than spike magnitudes alone.

4 Optimal Trading Strategy

A central objective of this section is to determine how large our virtual trading positions should be in each NYISO zone, once a directional signal has been generated by the spike–forecasting model. Correctly sizing trades is essential: although DART spreads create strong economic opportunities, large virtual positions mechanically shift the day-ahead clearing price through both system-level and zonal congestion effects. Hence, to maximize profitability while avoiding excessive market impact, we require an explicit model linking trade size to DA price response. The following subsections develop this scaling model, calibrate its parameters, and derive the optimal zonal quantities used in our strategy. For notational simplicity, we henceforth drop the market subscript m, as the analysis in this section focuses on NYISO.

4.1 Price Impact Model

Let Z denote the number of zones and let $q_t \in \mathbb{R}^Z$ be the vector of signed bidding quantities (MWh) at time t, where $q_{t,z} > 0$ represents an INC (virtual demand) in zone z at time t and $q_{t,z} < 0$ represents a DEC (virtual supply). For each hour t and zone z, denote

$$\mathrm{DA}_{t,z},\ \mathrm{RT}_{t,z} \in \mathbb{R}, \qquad \mathrm{DART}_{t,z} := \mathrm{DA}_{t,z} - \mathrm{RT}_{t,z}.$$

The \$-per–MWh trading edge of an INC or a DEC trade is then

$$r_{t,z}^{\mathrm{INC}} = -\,\mathrm{DART}_{t,z}, \qquad r_{t,z}^{\mathrm{DEC}} = +\,\mathrm{DART}_{t,z}.$$

9

If a trade of size $q \in \mathbb{R}$ is executed, the realized dollar P&L for side $s \in \{\text{INC}, \text{DEC}\}$ at time t in zone z is

$$\Pi_{t,z}^{(s)}(q) \;=\; q\Big(r_{t,z}^{(s)} - I(q,t,z)\Big), \tag{2}$$

where $I(q,t,z)$ is the \$-per-MWh price impact imposed on the DA price, depending on the submitted quantity, time and zone.

Before specifying the price–impact model, we recall the standard decomposition of day-ahead locational marginal prices (LMPs). In all U.S. ISOs, including NYISO, ISO–NE, and ERCOT [15, 12], the day-ahead price at zone z and hour t can be written as

$$\text{DA}_{t,z} = \text{Energy}_t + \text{Loss}_{t,z} + \text{Congestion}_{t,z}.$$

The energy component is system-wide, whereas losses and congestion vary across zones due to transmission constraints and network topology. These spatial components are precisely what generate cross-zonal heterogeneity in DART spreads and motivate a zone-dependent treatment of price impact in our scaling model.

Virtual demand and supply bids shift the residual demand curve and thus impact day ahead clearing prices. Following the standard approach [2, 10] in optimal execution and market impact models, see also [1] for a stochastic control formulation of optimal trading with price impact in electricity markets, we approximate the zonal response of prices to aggregate traded quantity S_t by a piecewise linear function, with energy-impact coefficients k_E^+ and k_E^-, and a separate linear impact from the trade size $q_{t,z}$ in the specific zone with coefficient k_z:

$$I(q,t,z) = \big(k_E^+ \mathbf{1}_{\{S_t \geq 0\}} + k_E^- \mathbf{1}_{\{S_t < 0\}}\big) S_t + k_z \, q_{t,z}, \qquad S_t := \sum_z q_{t,z}.$$

The motivation for the first term is that when $S_t > 0$, the system takes a net INC position and moves along the demand curve, whereas when $S_t < 0$ it takes a net DEC position and moves along the supply curve. Since the slopes of the supply and demand curves differ, their marginal price impacts differ as well, motivating the use of distinct energy-impact coefficients k_E^+ and k_E^-. We estimate these coefficients in Section 4.3 using aggregate supply and demand curve.

Moreover, zones in NYISO differ substantially in their typical demand levels and exposure to transmission constraints. Large demand centers such as NYC and Long Island tend to absorb incremental virtual positions with relatively small marginal effects on losses and congestion, whereas smaller or more constrained zones can exhibit much larger local price sensitivities. This motivates introducing a zone-specific local impact coefficient k_z, capturing how virtual demand or supply submitted bids in zone z affect the spatial components of day-ahead prices. In Section 4.4, we calibrate these coefficients using zonal load and price data.

4.2 Optimal zonal quantities with asymmetric energy impact

Each zone z is equipped with a classifier that outputs the probability $p_{t,z}$ that hour t in zone z experiences an INC spike (negative DART) or a DEC spike (positive DART). After

training on 2015–2019, we tune the decision thresholds τ_z on the 2020–2021 validation set. At time t, we trade in zone z whenever

$$p_{t,z} \geq \tau_z,$$

and select the trade direction (INC or DEC) with the larger predicted expected payoff.

Conditional on trading, we next determine the appropriate trade size in each zone. To this end, we estimate the conditional expected economic revenue on the validation period:

$$x_{t,z}^{\text{INC}} := \mathbb{E}\left[r_{t,z}^{\text{INC}} \mid p_{t,z} \geq \tau_z\right], \qquad x_{t,z}^{\text{DEC}} := \mathbb{E}\left[r_{t,z}^{\text{DEC}} \mid p_{t,z} \geq \tau_z\right]. \tag{3}$$

These zone-specific expected payoffs summarize how profitable INC and DEC trades tend to be when the model signals a spike and executes a trade. They form the input to the scaling optimization that determines the virtual position allocated to each zone.

Given a fixed time t and the selected trade direction, we collect the expected payoffs into the vector

$$x_t \equiv (x_{t,1}, \ldots, x_{t,Z}) \in \mathbb{R}^Z,$$

and choose zonal quantities $q_{t,z}$.

For a trade vector $q \in \mathbb{R}^Z$, we define the objective function

$$F(q) = x_t^\top q - \left(k_{\text{E}}^+ \mathbf{1}_{\{S \geq 0\}} + k_{\text{E}}^- \mathbf{1}_{\{S < 0\}}\right) S^2 - \sum_{z=1}^{Z} k_z q_z^2, \qquad S := \mathbf{1}^\top q, \tag{4}$$

which represents the expected price-impacted DART payoff of the trade q placed at time t. The energy impact coefficient is sign-dependent: we use k_{E}^+ when $S > 0$ (net buy) and k_{E}^- when $S < 0$ (net sell).

Fix k_{E} (either k_{E}^+ or k_{E}^-) and suppose the optimum is interior. The first-order conditions of (4) yield the following optimal zonal trade quantities:

$$q_{t,z}^\star = \frac{x_{t,z} - 2k_{\text{E}}S}{2k_z}. \tag{5}$$

Define

$$H := \sum_{z=1}^{Z} \frac{1}{k_z}, \qquad N_t := \sum_{z=1}^{Z} \frac{x_{t,z}}{k_z}.$$

Summing (5) over z yields the closed-form net position

$$S = \frac{N_t/2}{1 + k_{\text{E}}H}. \tag{6}$$

We therefore obtain two interior candidate solutions:

$$\text{INC regime } (S > 0): \quad S^{(+)} = \frac{N_t/2}{1 + k_{\text{E}}^+ H}, \qquad q_{t,z}^{(+)} = \frac{x_{t,z} - 2k_{\text{E}}^+ S^{(+)}}{2k_z},$$

$$\text{DEC regime } (S < 0): \quad S^{(-)} = \frac{N_t/2}{1 + k_{\text{E}}^- H}, \qquad q_{t,z}^{(-)} = \frac{x_{t,z} - 2k_{\text{E}}^- S^{(-)}}{2k_z}.$$

A third possibility is that the optimum lies on the boundary where the net position is zero, so that the energy impact term vanishes and only local impacts remain. In this regime we solve

$$\max_{q \in \mathbb{R}^Z} x_t^\top q - \sum_{z=1}^Z k_z q_z^2 \quad \text{subject to} \quad \mathbf{1}^\top q = 0. \tag{7}$$

Introducing a Lagrange multiplier, the optimal zonal trade quantities are given by

$$q_{t,z}^{(0)} = \frac{x_{t,z} - N_t/H}{2k_z}, \qquad S^{(0)} = 0.$$

The optimization therefore yields three candidate solutions $q_t^{(+)}, q_t^{(-)}, q_t^{(0)}$. We retain $q_t^{(+)}$ only when $S^{(+)} > 0$, and $q_t^{(-)}$ only when $S^{(-)} < 0$. The net-flat solution $q_t^{(0)}$ is always feasible. Among all admissible candidates, the optimal trading vector is the one that maximizes the objective value $F(q)$.

4.3 Estimating the energy-impact coefficients

We describe system-wide price formation in the NYISO Day-Ahead Market using aggregate supply and demand curves. Let $Q^S(p)$ and $Q^D(p)$ denote, respectively, the total quantity supplied and demanded at price p. For each hour t, the day-ahead clearing price $p^\star(t)$ satisfies

$$Q^S\big(p^\star(t)\big) = Q^D\big(p^\star(t)\big).$$

Equivalently, defining the cleared quantity

$$q^\star(t) := Q^S\big(p^\star(t)\big) = Q^D\big(p^\star(t)\big),$$

the relevant price–quantity relationship is given locally by the inverse supply and demand curves $P^S(q) := (Q^S)^{-1}(q)$ and $P^D(q) := (Q^D)^{-1}(q)$ evaluated at $(q^\star(t), p^\star(t))$. Our objective is to estimate the local slope of this mapping at the day-ahead equilibrium. Because the bid stack is observed only as a discrete collection of bids, we estimate these derivatives numerically using one-sided finite differences. This approach follows the bid-stack–based price formation framework introduced in [5], which model s electricity prices as arising from local properties of the aggregate supply and demand curves.

A net long day-ahead position of size $\Delta q > 0$ corresponds to an exogenous increase in aggregate demand. Operationally, the realized cleared quantity becomes

$$Q^S(p^+) = Q^D(p^+) = Q^D(p^\star) + \Delta q = Q^S(p^\star) + \Delta q,$$

where p^+ denotes the perturbed clearing price. Expanding Q^S to first order around $p^\star$ yields

$$p^+ - p^\star \approx \frac{\Delta q}{(Q^S)'(p^\star)} > 0. \tag{8}$$

Equivalently, this corresponds to a first-order expansion of the inverse supply curve $P^S(q)$ around $q^\star$. Thus the buy-side price impact is governed by the local slope of the aggregate supply curve.

Table 1: Average linear price impact $k_E^+(\$/1000\text{MWh})$ induced by a $+1000$ MWh demand shock, by season and load band: train (2015–2019) vs. test (2022–2025).

Season	Band	Top-10 spikes (2015–2019)	Top-10 spikes (2022–2025)
Winter	Off-Peak	17.03	10.56
Winter	Peak	23.21	26.27
Summer	Off-Peak	8.05	66.84
Summer	Peak	34.64	46.48
Shoulder	Off-Peak	1.74	2.34
Shoulder	Peak	10.48	22.23

We estimate k_{E}^+ by taking $\Delta q = 1000$ MWh and averaging the resulting finite-difference price responses across a selected set of hours within each season and Peak/Off-Peak bucket. Specifically, we consider the Top-10 spike hours ($N = 10$). The resulting average buy-side impacts are reported in Table 1.

Similarly, a net short position of size $\Delta q < 0$ corresponds to a shift along the inverse demand curve. In this case, the perturbed clearing price p^- satisfies

$$p^- - p^\star \approx \frac{\Delta q}{(Q^{\text{D}})'(p^\star)} < 0. \tag{9}$$

The sell-side impact is thus governed by the local slope of the aggregate demand curve. We estimate k_{E}^- analogously using one-sided finite differences with $\Delta q = 1000$ MWh and the same sampling scheme. Corresponding sell-side impacts are reported in Table 2.

Table 2: Average linear price impact $k_E^-(\$/1000\text{MWh})$ induced by a -1000 MWh supply shock, by season and load band: train (2015–2019) vs. test (2022–2025).

Season	Band	Top-10 spikes (2015–2019)	Top-10 spikes (2022–2025)
Winter	Off-Peak	-92.15	-117.95
Winter	Peak	-114.89	-131.33
Summer	Off-Peak	-19.73	-24.40
Summer	Peak	-45.82	-59.11
Shoulder	Off-Peak	-17.96	-22.78
Shoulder	Peak	-28.37	-32.44

The parameters $(k_{\text{E}}^+, k_{\text{E}}^-)$ should therefore be interpreted as local average slopes of the inverse residual supply and demand curves at the day-ahead clearing point. In general, they need not coincide: supply and demand can exhibit markedly different slopes near equilibrium, particularly during stressed system conditions. This naturally leads to an asymmetric price response to buy- versus sell-side shocks.

To capture systematic variation in these slopes, we stratify the estimation by season (Winter, Summer, Shoulder) and by load regime (Peak and Off-Peak hours), reflecting predictable changes in system stress and bid-stack geometry. In all subsequent optimization

experiments, the system-wide impact parameters (k_E^+, k_E^-) are estimated exclusively on the calibration sample (2015–2019) and treated as fixed inputs when constructing optimal portfolios and computing realized P&L over the out-of-sample test period (2022–2025). This procedure ensures that portfolio decisions rely solely on historically available information and that all reported profits are free of look-ahead bias. For illustration, in the calibration sample (2015–2019) the largest buy-side impact occurs during Summer Peak hours, where a $+1000$ MWh demand shock raises prices by 34.64 \$/MWh on average, while on the sell side, the largest impact is observed during Winter Peak hours, where a -1000 MWh supply shock lowers prices by 114.89 \$/MWh.

Figures 5 and 6 provide a visual illustration of the local linearity underlying this calibration. For a selection of representative hours, we plot the supply and demand curves in a neighborhood of the Day-Ahead Market intersection and compare the market-clearing price before and after an exogenous quantity shock. The dotted line in each panel corresponds to the local linear approximation used in the impact model, while the displacement between the pre- and post-shock clearing prices reflects the realized price response to the injected demand or supply. These examples illustrate how, at the relevant operating point, the bid stack is well-approximated by a linear slope, justifying the use of a linear impact specification and motivating the estimation of seasonal and load-regime–specific impact coefficients.
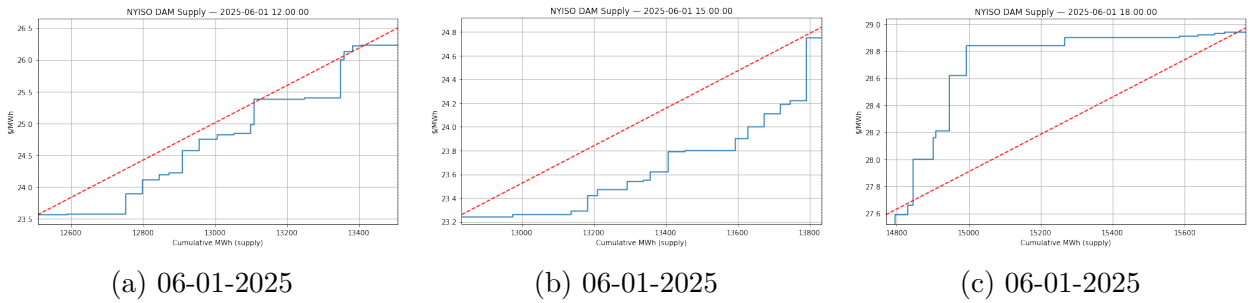
| (a) 06-01-2025 | (b) 06-01-2025 | (c) 06-01-2025 |

Figure 5: Supply stack and linear approximation near the DA price-setting intersection point at three different hours.

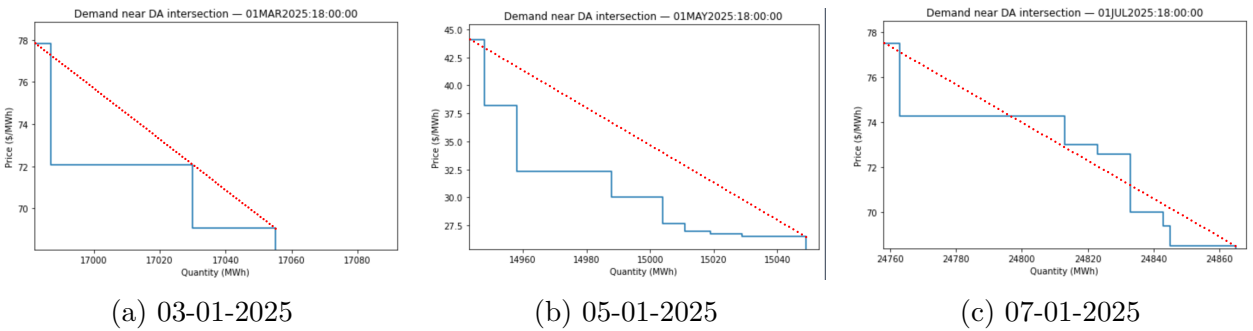| (a) 03-01-2025 | (b) 05-01-2025 | (c) 07-01-2025 |

Figure 6: Demand stack and linear approximation near the DA price-setting intersection point at three different hours.

4.4 Estimating local impact coefficients

To calibrate the zone-specific impact coefficients k_z, we estimate how forecast load affects zonal day-ahead prices in the NYISO market through the loss and congestion components of the locational marginal price (LMP). As a reference, we first focus on the Long Island (LONGIL) zone, which is both a large demand center and an import-constrained load pocket in NYISO. Its loss and congestion components reflect flows across multiple upstream interfaces and exhibit substantial non-local transmission stress, making Long Island a natural baseline for calibrating marginal price impact.

We regress the DA loss-minus-congestion component on the corresponding zonal forecast load separately for each zone, season, and Peak/Off-Peak bucket. The estimated slopes, reported in Table 12, measure the average price impact (in $/MWh) of a +1000 MWh increase in forecast load within that zone. In Long Island, the estimated impact ranges from 4.95 to 7.82 in Shoulder, from 5.06 to 17.73 in Summer, and from 43.30 to 43.63 in Winter, depending on the Peak/Off-Peak bucket.

Table 13 reports the corresponding average forecast load by zone and season over 2015–2021. Zones with higher typical loads (e.g., NYC and Long Island) tend to exhibit smaller marginal price impacts per MW, whereas smaller or more transmission-constrained zones (e.g., Millwood and Dunwoodie) show substantially higher sensitivities. These patterns are consistent with localized load shocks being diluted in large demand centers and amplified in smaller or constrained zones.

Guided by the regression evidence—most notably the relatively small marginal impacts in large zones such as Long Island and NYC [22, 14], and the much larger impacts in smaller or more constrained zones—we model the local linear impact coefficients k_z as inversely proportional to average zonal load. Using historical mean actual loads L_z over 2015–2021, we calibrate

$$k_z = k_{\text{LONGIL}} \frac{L_{\text{LONGIL}}}{L_z}, \qquad k_{\text{LONGIL}} = 0.050\$/(\text{MWh})^2,$$

so that the overall scale of the k_z is consistent with the order of magnitude of the Long Island Summer–Peak regression coefficients (shown in Figure 9 in the Appendix), while preserving the empirical ranking of zones by size and sensitivity. This yields the following estimates:

$$k_{\text{NYC}} = 0.020 \qquad k_{\text{LONGIL}} = 0.050 \qquad k_{\text{WEST}} = 0.067 \qquad k_{\text{CENTRL}} = 0.065,$$
$$k_{\text{CAPITL}} = 0.085 \qquad k_{\text{NORTH}} = 0.210 \qquad k_{\text{DUNWOD}} = 0.169 \qquad k_{\text{MILLWD}} = 0.357,$$
$$k_{\text{HUDVL}} = 0.105 \qquad k_{\text{MHKVL}} = 0.129 \qquad k_{\text{GENESE}} = 0.103.$$

Zones with larger average loads (e.g., NYC, LONGIL, CENTRL) therefore accommodate larger virtual positions with lower price impact, while smaller or more constrained zones (e.g., MILLWD and NORTH) exhibit higher sensitivity.

Finally, Table 14 reports average correlations between forecast load and the day-ahead loss and congestion components across zones. Both components are consistently positively correlated with forecast load across all seasons and time buckets, supporting the modeling assumption that higher forecasted load increases losses and congestion in expectation.

5 Performance in NYISO

This section evaluates the empirical performance of the proposed trading strategy when deployed in practice. All predictive models, impact parameters, and decision thresholds are fixed based on the calibration and validation samples, and performance is assessed out of sample on NYISO data from 2022–2025. In contrast to Section 4, which focuses on model construction and optimal trade sizing, the results reported here reflect the realized interaction between forecasting accuracy, market impact, and cross-zonal portfolio allocation.

If the expected return in the validation set 2020–2021 is negative, we do not consider bidding for this zone, since our model was not able to give a successful prediction. Table 3 suggests that we should not consider the North zone about INC predictions and the Long Island zone for the DEC predictions.

Table 3: Validation period (2020–2021): trade counts, average P&L (USD/MWh), and eligibility per zone.

Zone	INC Trades	INC Avg Win	DEC Trades	DEC Avg Win
NYC	122	12.35	326	3.46
LONGIL	316	38.12	1705	-1.07
WEST	152	5.21	307	9.76
CENTRL	36	2.26	61	17.41
CAPITL	75	0.63	206	11.00
NORTH	41	-0.13	25	6.48
DUNWOD	49	7.72	189	3.03
MILLWD	56	18.81	167	0.82
HUDVL	47	3.30	159	9.92
MHKVL	33	2.65	52	16.47
GENESE	40	12.25	51	13.75

Notably, the optimal strategy does not trade each zone in isolation. While the predictive model assigns to every zone–hour a directional signal (INC for negative predicted DART and DEC for positive predicted DART), the executed trades are determined jointly across zones. In particular, it may allocate a position whose sign differs from the local predicted direction. For example, it can place a DEC in one zone while taking an INC in another, even when both zones individually exhibit positive expected DART spreads. This behavior is driven by the system-wide impact penalty k_E: by taking offsetting positions, the strategy reduces aggregate exposure and associated costs, allowing risk to be concentrated in zones where marginal price impact is lowest.

As a result, a zone may exhibit negative realized P&L despite a correct directional prediction. To disentangle model accuracy from portfolio allocation effects, we therefore report results in two complementary views. The prediction view evaluates performance based solely on the model's directional signals, while the execution view reflects realized P&L after optimization and cross-zone balancing, where we can see the results in Figure 7.

Moreover, Table 15 reports zone-level performance, while Table 16 aggregates results across all zones for each test year.

(a) INC — execution view   (b) DEC — execution view

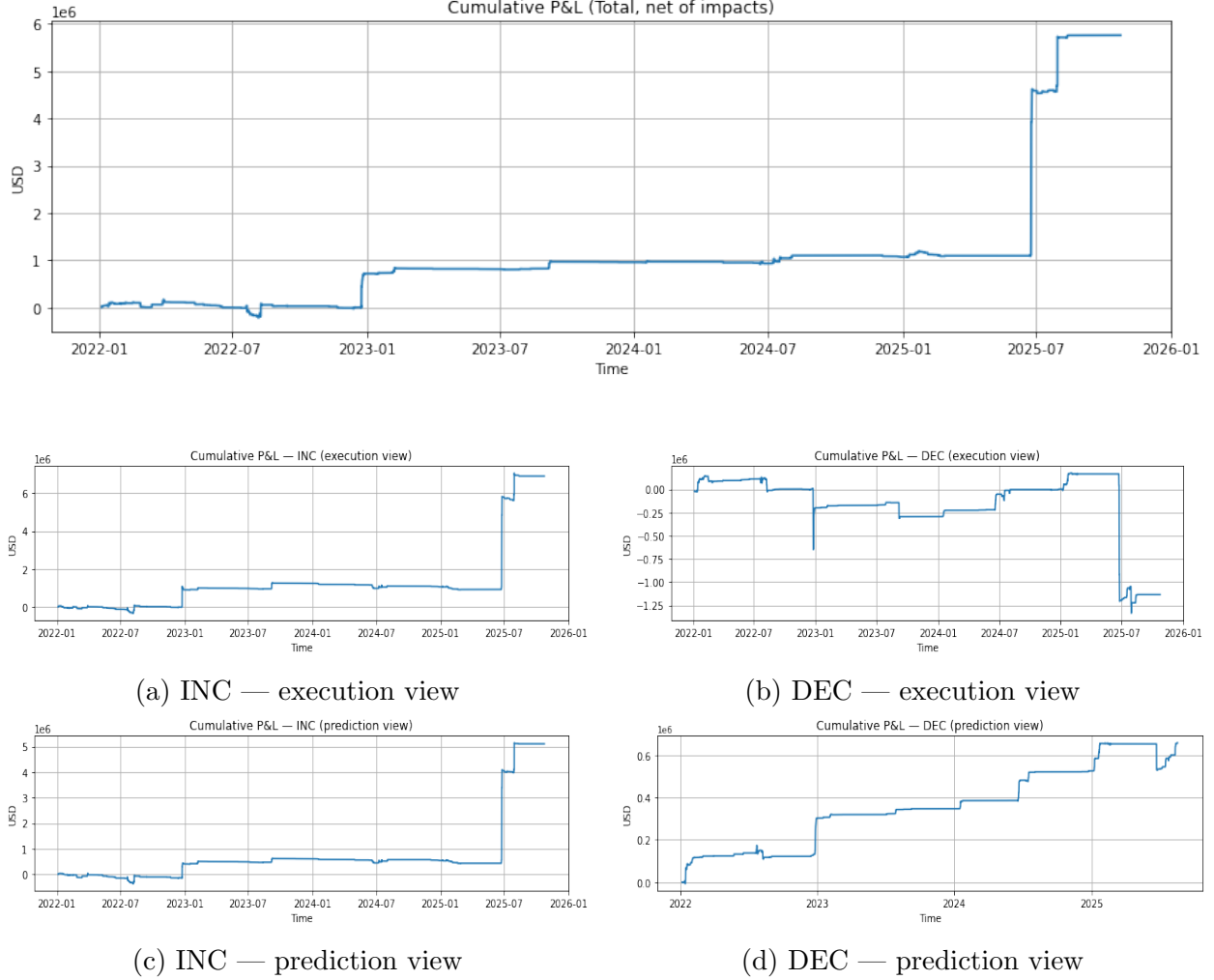(c) INC — prediction view   (d) DEC — prediction view

Figure 7: Cumulative P&L: total (top) and by side and attribution view (bottom). All values are in USD.

Table 4 reports, for each zone, the number of active trading hours, the average absolute position size, and the resulting P&L. The largest virtual positions are taken in Long Island, which is consistent with its market characteristics: the zone combines frequent and sizable DART spikes with high average load, implying a relatively low marginal price impact per traded MWh.

A further validation of our assumptions on the energy-impact coefficients k_{E} comes from examining trading hours in which the strategy takes its largest day-ahead positions. On 24 June 2025—the most profitable day in the out-of-sample period—the strategy repeatedly submits large net buy (INC) positions during Summer Peak hours. Using the NYISO bid stack for these same hours, we recompute the day-ahead clearing price after shifting the residual demand curve upward by the executed quantity q_t of MWh. This allows us to measure the realized one–sided price impact,

$$\Delta P_t \;=\; P_t^{\mathrm{DA}}(q_t) - P_t^{\mathrm{DA}},$$

17

Table 4: Per-zone attribution on the TEST period (2022–2025), execution view with dynamic $q^\star$ and price impacts.

Zone	Hours Active	Avg $|q|$ (MW)	P&L (USD)
LONGIL	571	118.70	6,004,480
NYC	1009	17.71	722,617
MILLWD	775	2.67	119,145
GENESE	397	8.91	118,976
WEST	1140	12.34	26,839
NORTH	160	3.32	-10,806
MHKVL	426	12.64	-101,829
DUNWOD	803	3.15	-169,380
CENTRL	440	27.54	-209,366
CAPITL	1026	14.34	-355,918
HUDVL	733	9.10	-384,604
Total / Stats:			**5,760,154**

and the corresponding empirical slope

$$\frac{\Delta P_t}{q_t} \times 1000 \qquad (\$/\text{MWh per 1000 MWh}).$$

The results in Table 17 show that the realized slopes lie between roughly 8 and 41$/MWh per 1000 MWh. These magnitudes are fully consistent with the calibrated Summer–Peak coefficients $k_{\mathrm{E}}^{+} \in [34.64, 46.48]/1000\text{MWh}$ obtained from the perturbation experiments in Section 4.3. Thus, the empirical price impact observed during the largest trading day strongly supports the validity of our linear approximation and our chosen parameter values.

5.1 Selective Spike Forecasting

On the 2022–2025 test period, the joint model exhibits a highly selective forecasting behavior, characterized by high precision but low recall, as we can see from Tables 18 and 19. Average precision is approximately 0.30 for INC trades and 0.77 for DEC trades, indicating relatively few false positives, while recall remains around 0.04–0.05, meaning that only a small fraction of all realized spike events is acted upon. This pattern reflects a profit-oriented design: the strategy trades only when the model assigns high confidence to extreme DART deviations, favoring signal quality over coverage.

To assess whether the model is selecting economically relevant spikes rather than arbitrary subsets of hours, Figures 10 and 11 compare the empirical distributions of realized DART spikes with those selected by the model. In each case, we compare both against the full sample of hours and against the largest spike quantiles. Across both hour-of-day and month-of-year dimensions, the model-selected distributions align much more closely with the largest observed spikes than with the unconditional sample.

This effect is quantified using the Jensen–Shannon (JS) divergence, a symmetric and bounded measure of dissimilarity between two probability distributions. Given distributions

P and Q on a common support, define their mixture $M = \frac{1}{2}(P+Q)$. The JS divergence is

$$\mathrm{JS}(P\|Q) = \frac{1}{2}\,\mathrm{KL}(P\|M) + \frac{1}{2}\,\mathrm{KL}(Q\|M)\,,$$

where $\mathrm{KL}(P\|Q) = \sum_x P(x)\log\!\big(\frac{P(x)}{Q(x)}\big)$ denotes the Kullback–Leibler divergence. We note that $\mathrm{JS}(P\|Q) \in [0, \log 2]$, with smaller values indicating more similar distributions [18].

In particular,

$$\textbf{INC:}\quad \mathrm{JS}_{\text{top 20\%}} = 0.039 \quad \text{vs.} \quad \mathrm{JS}_{\text{all}} = 0.094,$$
$$\textbf{DEC:}\quad \mathrm{JS}_{\text{top 5\%}} = 0.061 \quad \text{vs.} \quad \mathrm{JS}_{\text{all}} = 0.116.$$

The substantially smaller divergences for the top spike quantiles show that predicted trading hours are statistically closer to the most extreme realized price deviations than to typical hours. In other words, although the model captures only a small fraction of all spikes, it disproportionately targets events that resemble the largest historical DART dislocations, consistent with the subsequent profitability of the trading strategy.

5.2 Enforcing Directional Consistency

In the baseline strategy, the portfolio optimizer is free to choose the sign of the zonal position $q_{t,z}$ so long as the resulting expected revenue (after impact) is positive. As a consequence, a zone can end up with an executed DEC position even in hours where the spike–forecasting model indicates a negative DART (and hence an INC position), or vice versa, because the optimizer may use offsetting positions across zones to reduce system-wide impact costs. To enforce a tighter link between forecasts and execution, we introduce a side-clipping rule: at each zone–hour we retain only the signal consistent with the predicted DART sign (INC if the model predicts negative DART, DEC if it predicts positive DART), and set all conflicting signals to zero before testing the strategy. This mechanism forces each traded hour to take positions only in the direction implied by the model's sign prediction, while still allowing the optimizer to choose the trade size.

Figure 13 shows that this clipped strategy performs better on the 2022–2025 test set. The total P&L increases relative to the unconstrained optimizer, and both the INC and DEC components become smoother and less noisy.

Table 23 reports the per-zone attribution of the clipped strategy. Restricting trades to the model-consistent direction reduces the number of active hours in some zones, but the remaining positions tend to have higher average profitability. Long Island remains the dominant contributor, followed by New York City and Capital, reflecting the strength of DEC trades in these load pockets.

Overall, the clipped strategy preserves most of the performance of the full optimizer while improving interpretability and robustness. By aligning trades strictly with the predicted sign of DART, it reduces contradictory positions and produces a cleaner mapping between forecasts and executed trades.

5.3 Restricting the Strategy to Statistically Significant Buckets

We revisit the previous strategy. However, now we split the evaluate our model by seasonality (Winter/Summer/Shoulder months)- and Peak/Off-Peak hours. Then, we restrict

attention to zone–season–band buckets that exhibit statistically significant performance in the validation period (2020–2021). Specifically, we retain only those buckets whose mean P&L has a t-statistic exceeding 2 and the number of trades is at least 50, corresponding approximately to 95% confidence against a zero-mean null.

Under this restriction, the universe of traded zones shrinks substantially, as Tables 21 and 22 suggest. On the INC side, only Long Island satisfies the significance criterion, whereas on the DEC side the retained zones are Capital, Central, Long Island, New York City, and West. All other zone–band combinations are excluded from trading in the test period.

Figure 12 reports cumulative P&L over 2022–2025 for this restricted strategy. As expected, total profits are slightly lower than in the fully pooled specification, reflecting the reduced number of traded positions. Nevertheless, performance remains strong, with the majority of gains concentrated during the large summer 2025 spike episodes.

To assess predictive accuracy, Table 20 summarizes the fraction of trades that coincide with realized spikes and the frequency with which the sign of the DART spread is correctly predicted. On the INC side, approximately 27% of trades occur during realized positive spikes, and the model predicts the correct sign in 41% of hours. By contrast, DEC predictions are substantially more reliable: roughly 76% of DEC trades coincide with negative spikes, and nearly 80% correctly predict the spread sign.

Overall, this analysis highlights the asymmetry between INC and DEC signals that we previously saw on Section 5.1: while INC opportunities are sparse and harder to time reliably, DEC signals exhibit both stronger statistical persistence and significantly higher predictive accuracy, consistent with the validation-period evidence.

6   Conclusion

This paper analyzes day-ahead versus real-time (DART) spreads in U.S. organized wholesale electricity energy markets operated by Independent System Operators (ISOs), and extends the framework of [9] in three main directions: multi-zone spike forecasting, an explicitly calibrated price–impact model, and the optimal scaling of virtual positions. Working with NYISO, ISO–NE, and ERCOT, we construct leakage-free feature sets that respect each ISO's day-ahead bid deadline and estimate zone-specific logistic regressions for both positive and negative DART spikes. The resulting models are deliberately selective: they trade only when assigned high spike probabilities, thereby prioritizing economic relevance over statistical coverage.

Our empirical results show that spike predictability is highly heterogeneous across markets and zones. In ISO–NE and ERCOT, DART spreads are almost perfectly synchronized across load zones, so a single representative node captures nearly all useful variation. By contrast, NYISO exhibits much weaker and more dispersed cross–zone correlations, driven by localized congestion and loss patterns. In this environment, multi-zone modelling is essential: different zones deliver structurally different DART distributions and support distinct INC/DEC opportunities. Long Island emerges as the most profitable load pocket, combining frequent extreme spreads with high average load, while several upstate zones offer weaker but still statistically significant signals.

A central contribution of the paper is to move beyond unit-sized, impact-free backtests

and to construct an economically consistent link between trade size and expected price response. Using historical day-ahead bid stacks, we estimate system-wide energy impact coefficients and zone-specific congestion sensitivities, yielding a linear–quadratic impact model for virtual load. Closed-form expressions for the optimal zonal quantities show that portfolio-level decisions are shaped not only by local expected revenues, but also by cross-zone interactions through the common energy component. In particular, it can be optimal to take offsetting positions across zones in order to concentrate risk where marginal price impact is lowest. Backtests that ignore this feedback either overstate achievable profits or implicitly assume unrealistically small position sizes.

From a trading perspective, the most stable opportunities arise on the DEC side. Positive DART spikes (which generate DEC profits) occur more frequently and with greater statistical regularity, and the forecasting model identifies these events with higher precision. In contrast, INC opportunities—driven by negative DART spikes—are substantially more lucrative when they occur, but they are rarer, more volatile, and more sensitive to threshold selection and market-impact assumptions. As a result, DEC strategies deliver smoother and more persistent returns, whereas INC strategies contribute occasional but very large profit bursts. Restricting trades to directions consistent with the model's sign prediction and to statistically significant zone–season–band buckets preserves most of the economic value while improving robustness and interpretability.

Several extensions of this study offer promising directions for further research. First, the backtesting framework could be enriched by replacing our linear impact proxy with realized day-ahead price perturbations computed directly from historical bid stacks, thereby evaluating the strategy under the true system response rather than a parametric approximation. Second, more expressive structural models of market impact—for example, piecewise-linear, nonlinear, or congestion-regime–dependent formulations—may better capture the heterogeneity of supply curves across zones and seasons. Third, the economic value of the spike forecasts could be explored through alternative financial instruments beyond virtual INC/DEC trades, such as Financial Transmission Rights (FTRs) or other hedging products that monetize congestion patterns. Together, these extensions would move the methodology closer to a full market-consistent execution framework and broaden its applicability across different trading environments.

References

[1] René Aïd, Pierre Gruet, and Huyên Pham. An optimal trading problem in intraday electricity markets. *Mathematics and Financial Economics*, 10(1):49–85, 2016.

[2] Robert Almgren and Neil Chriss. Optimal execution of portfolio transactions. *Journal of Risk*, 3(2):5–39, 2001.

[3] Severin Borenstein, James B. Bushnell, and Frank A. Wolak. Measuring market inefficiencies in California's restructured wholesale electricity market. *American Economic Review*, 92(5):1376–1405, December 2002.

[4] Thomas M Christensen, Stan Hurn, and Kevin Lindsay. Forecasting spikes in electricity prices. *International Journal of Forecasting*, 28(2):400–411, 2012.

[5] Michael Coulon and Sam Howison. Stochastic behaviour of the electricity bid stack: From fundamental drivers to power prices. *The Journal of Energy Markets*, 2(1):29–69, 2009.

[6] Michael Coulon, Warren B. Powell, and Ronnie Sircar. A model for hedging load and price risk in the Texas electricity market. *Energy Economics*, 40:976–988, 2013.

[7] Electric Reliability Council of Texas. ERCOT market data. https://www.ercot.com, 2025. Accessed for Day-Ahead and Real-Time prices, load forecasts, and market data.

[8] Anthony Forgetta, Frédéric Godin, and Maciej Augustyniak. Distributional forecasting of electricity DART spreads with a covariate-dependent mixture model. *Energy Economics*, 144:108332, 2025.

[9] Rémi Galarneau-Vincent, Geneviève Gauthier, and Frédéric Godin. Foreseeing the worst: Forecasting electricity DART spikes. *Energy Economics*, 119:1–18, 2023.

[10] Jim Gatheral. No-dynamic-arbitrage and market impact. *Quantitative Finance*, 10(7):749–759, 2010.

[11] Trevor Hastie, Robert Tibshirani, and Jerome Friedman. *The Elements of Statistical Learning: Data Mining, Inference, and Prediction*. Springer, 2 edition, 2009.

[12] ISO New England. FAQs: Locational marginal pricing, 2025. Accessed: 2025-03.

[13] ISO New England. ISO New England markets and operations data. https://www.iso-ne.com/markets-operations/markets, 2025. Accessed for Day-Ahead and Real-Time prices, load forecasts, and market data.

[14] Kelly Stegmann, Mathangi Srinivasan Kumar, and Gina E. Craan. Congestion price component. Technical report, New York Independent System Operator (NYISO), September 2025. LBMP In-Depth Course, Remote Learning.

[15] Mathangi Srinivasan Kumar. *Locational Based Marginal Pricing*. New York Independent System Operator (NYISO), October 2025. New York Market Orientation Course (NYMOC), Rensselaer, NY.

[16] Jesus Lago, Grzegorz Marcjasz, Bart De Schutter, and Rafał Weron. Forecasting day-ahead electricity prices: A review of state-of-the-art algorithms, best practices and an open-access benchmark. *Applied Energy*, 293:116983, 2021.

[17] Dominik Liebl. Modeling and forecasting electricity spot prices: A functional data perspective. *The Annals of Applied Statistics*, 7(3):1562–1592, 2013.

[18] Jianhua Lin. Divergence measures based on the Shannon entropy. *IEEE Transactions on Information Theory*, 37(1):145–151, 1991.

[19] Francis A Longstaff and Ashley W Wang. Electricity forward prices: A high-frequency empirical analysis. *Journal of Finance*, 59(4):1877–1900, 2004.

[20] New York Independent System Operator. NYISO market data. `https://www.nyiso.com`, 2025. Accessed for Day-Ahead and Real-Time prices, load forecasts, and market data.

[21] Jakub Nowotarski, Eran Raviv, Stefan Trück, and Rafał Weron. An empirical comparison of alternative schemes for combining electricity spot price forecasts. *Energy Economics*, 46:395–412, 2014.

[22] NYISO. Locational minimum installed capacity requirements study for the 2024–2025 capability year. Technical report, New York Independent System Operator (NYISO), December 2024.

[23] Harmanjot Singh Sandhu, Liping Fang, and Ling Guan. Forecasting day-ahead price spikes for the ontario electricity market. *Electric Power Systems Research*, 141:450–459, 2016.

[24] Xuesong Wang, Sharaf K. Magableh, Oraib Dawaghreh, Caisheng Wang, Jiaxuan Gong, Zhongyang Zhao, and Michael H. Liao. Deep learning-based electricity price forecast for virtual bidding in wholesale electricity market, 2024.

A   Appendix

A.1   Tables and Figures for NYISO

Table 5: NYISO: per-year P&L by zone (INC only benchmark strategy)

Year	CAPITL	CENTRL	LONGIL	NORTH	NYC	WEST
2022	17,855	14,673	22,315	11,632	16,254	1,457
2023	-886	-353	3,163	-2,559	-2,582	679
2024	-1,383	371	3,065	754	3,966	454
2025	8,731	7,409	24,445	1,776	23,035	5,162
Total	24,316	22,099	52,988	11,602	40,673	7,752

Table 6: NYISO: per-year P&L by zone (DEC only benchmark strategy)

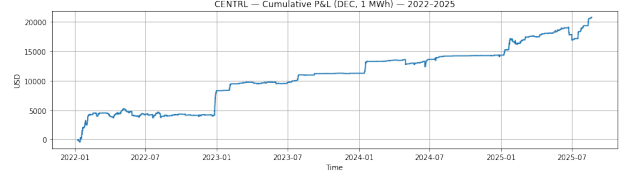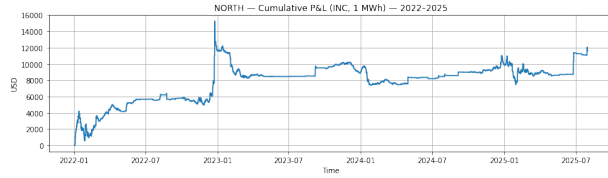| Year	CAPITL	CENTRL	LONGIL	NORTH	NYC	WEST
2022	10,749	8,287	6,879	6,427	8,705	6,082
2023	5,299	2,970	3,035	960	3,782	4,011
2024	6,288	3,057	5,020	2,135	2,425	2,100
2025	15,880	6,454	1,769	2,728	1,932	4,322
Total	38,215	20,768	16,703	12,250	16,844	16,516
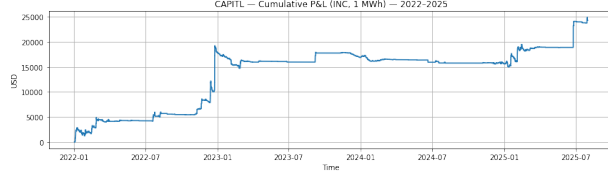
(a) CAPITL — INC
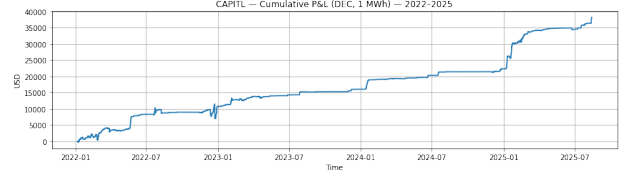
(b) CAPITL — DEC

(c) CENTRL — INC

(d) CENTRL — DEC

(e) NORTH — INC
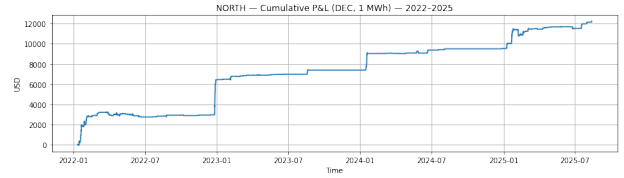
(f) NORTH — DEC
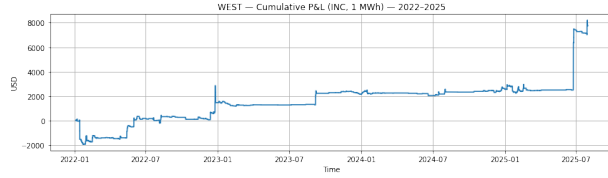
(g) WEST — INC
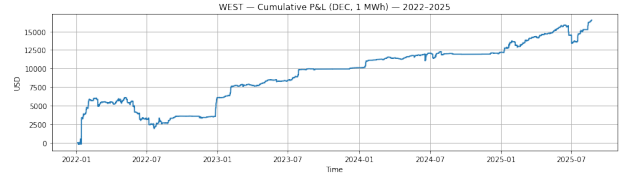
(h) WEST — DEC

Figure 8: NYISO: cumulative P&L by zone for remaining regions under the INC/DEC benchmark strategy.

Table 7: NYISO: yearly mean of DART spreads by zone

Year	CAPITL	CENTRL	LONGIL	NORTH	NYC	WEST
2015	0.33	0.27	1.09	0.25	0.54	-1.82
2016	0.67	0.20	0.67	0.25	-0.02	-0.13
2017	0.47	-0.11	1.40	1.27	0.90	-0.31
2018	-0.17	-0.49	0.80	-0.54	-1.02	-0.01
2019	1.06	0.48	-0.56	-0.11	0.71	-0.29
2020	-0.08	-0.10	-0.08	-0.60	-0.60	-0.03
2021	0.40	0.33	-0.84	-0.79	0.03	0.08
2022	-2.51	-2.10	-2.37	-1.56	-2.80	0.58
2023	1.76	0.29	-0.29	1.02	0.47	1.27
2024	1.38	0.54	1.20	0.06	-0.09	0.95
2025	1.62	-0.68	-3.18	-0.14	-4.05	0.50

A.2 DART Correlation Across Zones

Table 8: Correlation of DART spikes across NYISO zones (2015–2025)

	CAPITL	CENTRL	DUNWOD	GENESE	HUDVL	LONGIL	MHKVL	MILLWD	NORTH	NYC	WEST
CAPITL	1.00	0.71	0.78	0.69	0.87	0.60	0.72	0.83	0.47	0.75	0.56
CENTRL	0.71	1.00	0.78	0.99	0.86	0.62	0.99	0.83	0.74	0.76	0.81
DUNWOD	0.78	0.78	1.00	0.76	0.90	0.75	0.78	0.97	0.53	0.97	0.61
GENESE	0.69	0.99	0.76	1.00	0.84	0.61	0.98	0.81	0.73	0.74	0.80
HUDVL	0.87	0.86	0.90	0.84	1.00	0.71	0.86	0.96	0.59	0.88	0.68
LONGIL	0.60	0.62	0.75	0.61	0.71	1.00	0.62	0.74	0.42	0.73	0.48
MHKVL	0.72	0.99	0.78	0.98	0.86	0.62	1.00	0.83	0.78	0.76	0.79
MILLWD	0.83	0.83	0.97	0.81	0.96	0.74	0.83	1.00	0.57	0.94	0.65
NORTH	0.47	0.74	0.53	0.73	0.59	0.42	0.78	0.57	1.00	0.52	0.56
NYC	0.75	0.76	0.97	0.74	0.88	0.73	0.76	0.94	0.52	1.00	0.59
WEST	0.56	0.81	0.61	0.80	0.68	0.48	0.79	0.65	0.56	0.59	1.00

Table 9: Correlation of DART spreads across ISO–NE zones (2018–2025).

Region	CT	ME	NEMASS	NH	RI	SEMASS	VT	WCMASS
CT	1.000	0.988	0.995	0.996	0.995	0.995	0.999	0.998
ME	0.988	1.000	0.993	0.994	0.993	0.993	0.990	0.993
NEMASS	0.995	0.993	1.000	0.999	0.999	0.999	0.995	0.998
NH	0.996	0.994	0.999	1.000	0.999	0.999	0.997	0.999
RI	0.995	0.993	0.999	0.999	1.000	1.000	0.996	0.999
SEMASS	0.995	0.993	0.999	0.999	1.000	1.000	0.996	0.999
VT	0.999	0.990	0.995	0.997	0.996	0.996	1.000	0.999
WCMASS	0.998	0.993	0.998	0.999	0.999	0.999	0.999	1.000

Table 10: Correlation matrix of DART across ERCOT zones (2018–2025).

Zone	**NORTH**	**SOUTH**	**WEST**	**HOUSTON**
NORTH	1.000	0.991	0.998	0.980
SOUTH	0.991	1.000	0.991	0.981
WEST	0.998	0.991	1.000	0.978
HOUSTON	0.980	0.981	0.978	1.000

A.3 NYISO, ISO–NE & ERCOT Quantiles

Table 11: Empirical DART quantiles (USD/MWh) on the training sets for NYISO LONGIL, ISO–NE ME, and ERCOT WEST.

Quantile	LONGIL (NYISO)	ME (ISO–NE)	WEST (ERCOT)
$Q_{0.00}$	-2434.97	-109.17	-5891.08
$Q_{0.01}$	-121.57	-29.60	-77.20
$Q_{0.05}$	-34.95	-13.39	-13.74
$Q_{0.10}$	-16.33	-7.10	-7.65
$Q_{0.25}$	-3.09	-1.51	-2.02
$Q_{0.50}$	3.98	1.33	0.97
$Q_{0.75}$	11.21	4.62	4.96
$Q_{0.90}$	20.27	9.31	11.39
$Q_{0.95}$	29.18	14.03	17.39
$Q_{0.99}$	58.25	27.75	40.39
$Q_{1.00}$	1506.76	69.03	7675.51

A.4 Figures and Tables for the Optimal Trading Strategy

This subsection collects supplementary calibration results, diagnostic plots, and robustness checks underlying the trading strategy in Section 4. It includes (i) price–impact estimates by season and load band, (ii) validation and test–set execution diagnostics, and (iii) additional performance breakdowns and distributional comparisons.

Table 12: (Loss – Congestion) impact on LMP for a +1000 MW zonal load change ($/MWh), 2015–2021.

Zone	Shoulder		Summer		Winter	
	Off-Peak	Peak	Off-Peak	Peak	Off-Peak	Peak
CAPITL	8.56	2.36	−7.86	0.86	63.41	79.54
CENTRL	2.61	2.87	−0.37	2.39	4.16	4.56
DUNWOD	3.61	9.36	−5.20	11.39	111.28	104.13
GENESE	1.76	1.70	−0.41	1.21	1.49	0.04
HUDVL	9.51	5.91	−3.51	5.04	68.75	65.51
LONGIL	4.95	7.82	5.06	17.73	43.63	43.30
MHKVL	5.30	4.86	−0.37	4.21	13.18	18.27
MILLWD	52.70	46.17	−11.37	25.69	189.06	192.38
NORTH	0.26	3.80	−19.55	−44.72	−2.82	−0.91
NYC	−0.25	1.29	−0.05	2.18	13.21	12.29
WEST	1.88	14.36	−0.54	25.73	1.54	1.11

Table 13: Average forecast load (MW) by zone, season, and Peak/Off-Peak, 2015–2021.

|	Shoulder		Summer		Winter	
Zone	Off-Peak	Peak	Off-Peak	Peak	Off-Peak	Peak
CAPITL	1,133.2	1,336.2	1,330.3	1,645.6	1,294.1	1,486.9
CENTRL	1,503.0	1,785.7	1,629.5	2,041.0	1,728.3	2,003.5
DUNWOD	542.8	676.9	706.1	906.1	597.4	720.3
GENESE	918.8	1,124.1	1,057.9	1,367.4	1,023.3	1,220.3
HUDVL	879.3	1,053.3	1,073.4	1,376.3	1,012.0	1,172.0
LONGIL	1,887.4	2,327.4	2,636.2	3,435.6	2,061.7	2,462.3
MHKVL	632.3	767.0	674.4	866.9	786.5	925.6
MILLWD	250.4	309.6	309.2	404.6	305.3	362.5
NORTH	499.4	532.5	484.8	531.3	586.6	619.9
NYC	4,819.9	6,102.0	6,307.2	7,926.5	5,074.9	6,249.1
WEST	1,479.6	1,734.2	1,637.3	2,004.4	1,624.4	1,872.3
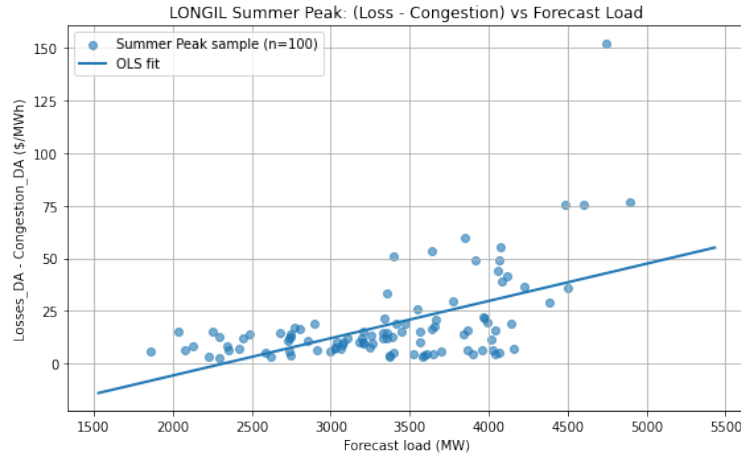
Figure 9: Scatter of (Forecasted Load,Loss+Congestion) for 100 random Summer–Peak hours in LONGIL.

Table 14: Average correlations across NYISO zones between forecast load and DA congestion/loss components, by season and Peak/Off-Peak bucket (2015–2021).

Season – Bucket	Corr(Forecast Load, Losses$_{DA}$)	Corr(Forecast Load, Congestion$_{DA}$)
Shoulder – Off-Peak	0.317	0.050
Shoulder – Peak	0.373	0.073
Summer – Off-Peak	0.352	0.112
Summer – Peak	0.397	0.177
Winter – Off-Peak	0.314	0.239
Winter – Peak	0.274	0.238

Table 15: Execution-view P&L by zone, aggregated over 2022–2025 (USD).

Zone	INC (Exec)	DEC (Exec)	Total
CAPITL	-6,564	-349,354	-355,918
CENTRL	-3,052	-206,313	-209,365
DUNWOD	-38,177	-131,202	-169,379
GENESE	49,801	69,174	119,975
HUDVL	-3,023	-411,510	-414,533
LONGIL	6,004,479	0	6,004,479
MHKVL	-1,178	-101,653	-102,831
MILLWD	128,091	-8,946	119,145
NORTH	-14,361	3,556	-10,805
NYC	778,698	-56,080	722,618
WEST	685	26,153	26,838

Table 16: Yearly total P&L by view and side (USD).

Year	INC (Exec)	DEC (Exec)	INC (Pred)	DEC (Pred)	Total (Pred)
2022	915,311	-201,181	411,226	302,904	714,130
2023	336,339	-93,707	198,424	44,207	242,631
2024	-185,819	296,156	-68,264	178,601	110,337
2025	5,829,911	-1,136,856	4,560,358	132,698	4,693,055

Table 17: Realized day-ahead price impact on 24 June 2025 for the executed net INC portfolio and the corresponding DART in Long Island (NYISO, upward shift of residual demand by q_t MWh).

Hour	q_t	P_t^{DA}	$P_t^{\mathrm{DA}}(q_t)$	ΔP_t ($/MWh)	$1000\,\Delta P_t/q_t$	DART
15:00	72.60	209.41	210.92	1.51	20.80	$-1{,}159.57$
16:00	85.90	222.59	224.79	2.20	25.61	-934.65
17:00	159.90	250.58	255.90	5.32	33.27	$-3{,}725.93$
18:00	163.10	224.79	226.59	1.80	11.04	$-4{,}372.52$
19:00	163.80	201.72	203.14	1.42	8.67	$-1{,}798.57$
20:00	161.30	170.00	176.57	6.57	40.73	-534.26
21:00	134.20	153.00	155.00	2.00	14.90	-145.64

Table 20: Prediction quality on the 2022–2025 test set for the restricted strategy.

Side	Trades	Spikes	Correct sign
INC	571	154 (27.0%)	232 (40.6%)
DEC	2720	2065 (75.9%)	2173 (79.9%)

Table 18: TEST precision/recall/F1 by zone for INC predicted.

zone	precision	recall	f1	TP	FP	FN	TN	support_pos	N
LONGIL	0.270	0.066	0.107	154	417	2167	29250	2321	31988
WEST	0.216	0.063	0.097	71	257	1064	30572	1135	31964
NYC	0.291	0.047	0.080	75	183	1535	30171	1610	31964
MILLWD	0.323	0.042	0.075	63	132	1430	31851	1493	33476
CAPITL	0.309	0.041	0.072	73	163	1714	30014	1787	31964
HUDVL	0.302	0.041	0.072	57	132	1347	31940	1404	33476
DUNWOD	0.309	0.040	0.071	60	134	1433	31849	1493	33476
CENTRL	0.310	0.035	0.063	45	100	1230	30589	1275	31964
GENESE	0.314	0.034	0.062	43	94	1206	32133	1249	33476
MHKVL	0.295	0.033	0.060	44	105	1276	32051	1320	33476
NORTH	0.343	0.030	0.056	49	94	1564	30281	1613	31988

Table 19: TEST precision/recall/F1 by zone for DEC predicted.

zone	precision	recall	f1	TP	FP	FN	TN	support_pos	N
LONGIL	0.645	0.146	0.238	2035	1118	11902	16933	13937	31988
WEST	0.747	0.059	0.110	635	215	10086	21028	10721	31964
CAPITL	0.795	0.052	0.098	635	164	11584	19581	12219	31964
NYC	0.722	0.050	0.093	560	216	10723	20465	11283	31964
DUNWOD	0.782	0.040	0.077	480	134	11386	21476	11866	33476
MILLWD	0.776	0.038	0.073	453	131	11383	21509	11836	33476
HUDVL	0.801	0.037	0.071	442	110	11466	21458	11908	33476
CENTRL	0.786	0.023	0.046	235	64	9795	21870	10030	31964
MHKVL	0.796	0.020	0.040	223	57	10675	22521	10898	33476
GENESE	0.792	0.020	0.039	209	55	10338	22874	10547	33476
NORTH	0.776	0.013	0.025	125	36	9725	22102	9850	31988

Table 23: Per-zone attribution of the clipped strategy on the 2022–2025 test set (execution view).

| Zone	Active hours	Avg. $|q|$ (MW)	P&L (USD)
LONGIL	570	118.91	5,692,023
NYC	464	21.92	910,936
CAPITL	777	10.10	303,353
WEST	807	9.89	242,054
CENTRL	235	23.66	189,883
MILLWD	184	6.23	147,420
GENESE	254	10.27	115,452
MHKVL	216	10.60	90,960
HUDVL	445	5.50	57,758
NORTH	28	5.93	3,531
DUNWOD	57	4.06	-1,143
Total	4,037	26.81 (w. avg.)	**7,752,227**
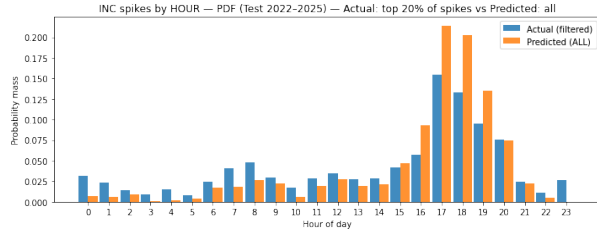
(a) INC — Actual top 20% vs. predicted
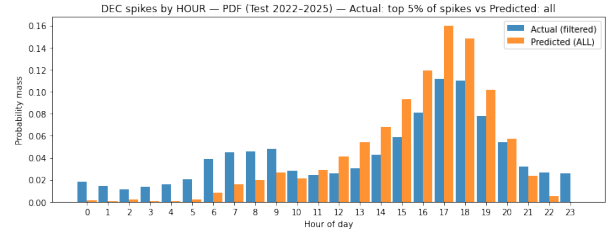
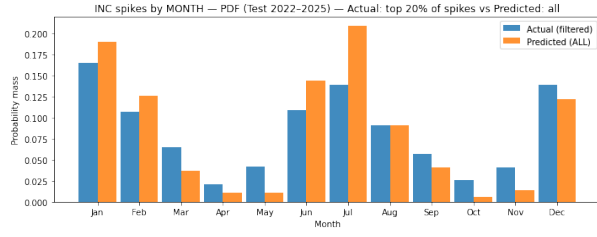(b) DEC — Actual top 5% vs. predicted
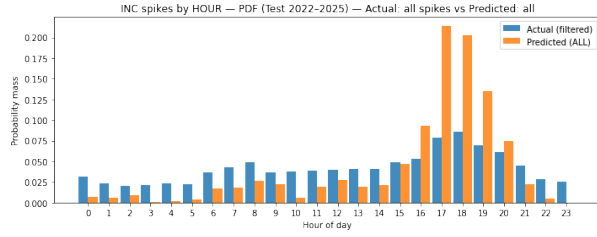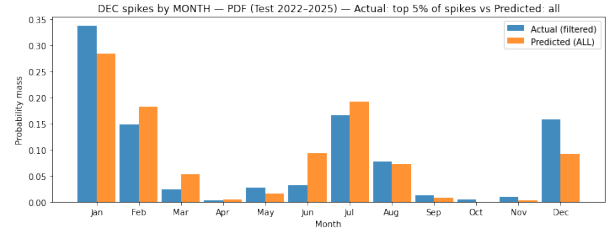
(c) INC — All hours vs. predicted
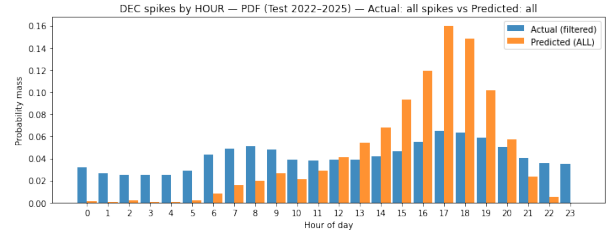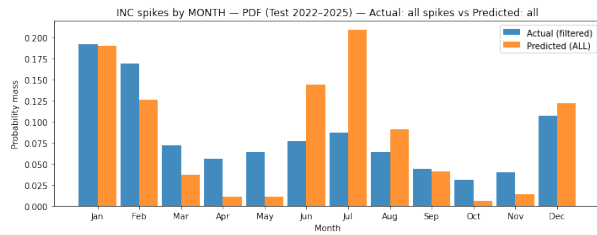
(d) DEC — All hours vs. predicted

Figure 10: Predicted vs. realized spike PDFs across **hour of day** (test period 2022–2025).
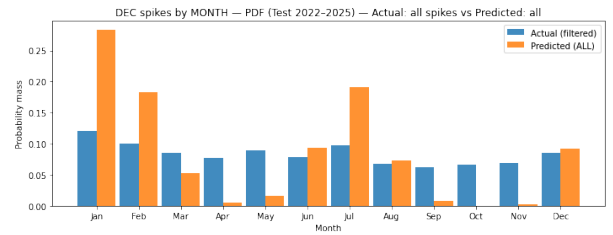

(a) INC — Actual top 20% vs. predicted

(b) DEC — Actual top 5% vs. predicted

(c) INC — All months vs. predicted

(d) DEC — All months vs. predicted

Figure 11: Predicted vs. realized spike PDFs across month of year (test period 2022–2025).
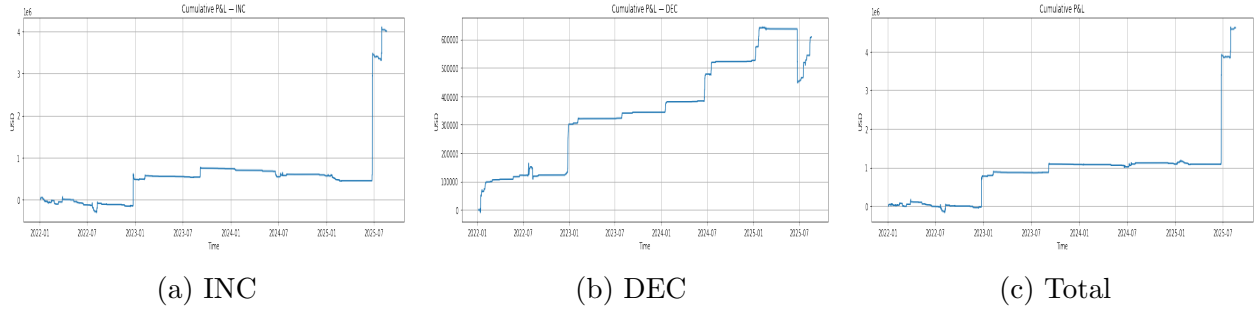
(a) INC (b) DEC (c) Total

Figure 12: Cumulative P&L for the restricted (statistically significant) strategy, test period 2022–2025.

Table 21: VALID 2020–2021, INC side: mean P&L (USD/MWh) and number of trades by zone, season and band.

Zone	W P	W O	Su P	Su O	Sh P	Sh O
CAPITL	16.24 (11)	–	-5.75 (57)	–	28.11 (7)	–
CENTRL	-3.82 (5)	–	-2.04 (26)	–	30.73 (5)	–
DUNWOD	6.43 (7)	–	4.95 (36)	–	25.85 (6)	–
GENESE	-4.32 (5)	–	17.47 (31)	–	-7.44 (4)	–
HUDVL	15.17 (6)	–	-2.50 (36)	–	30.81 (5)	–
LONGIL	19.20 (47)	–	44.50 (246)	–	8.60 (23)	–
MHKVL	-3.73 (5)	–	-1.32 (24)	–	34.43 (4)	–
MILLWD	7.61 (7)	–	19.64 (43)	–	25.95 (6)	–
NORTH	-9.10 (6)	–	-2.34 (31)	–	30.43 (4)	–
NYC	4.31 (8)	–	12.30 (107)	–	22.37 (7)	–
WEST	3.08 (19)	–	5.96 (116)	–	2.46 (17)	–

Table 22: VALID 2020–2021, DEC side: mean P&L (USD/MWh) and number of trades by zone, season and band.

Zone	W P	W O	Su P	Su O	Sh P	Sh O
CAPITL	27.94 (50)	–	6.24 (149)	–	-8.64 (7)	–
CENTRL	41.40 (7)	21.82 (1)	14.06 (51)	–	16.52 (2)	–
DUNWOD	29.13 (48)	–	-6.55 (134)	–	7.45 (7)	–
GENESE	36.22 (5)	22.67 (1)	11.26 (43)	–	6.71 (2)	–
HUDVL	31.37 (29)	–	4.93 (125)	–	10.36 (5)	–
LONGIL	1.89 (814)	49.54 (5)	-7.50 (655)	–	5.61 (231)	–
MHKVL	43.09 (7)	23.22 (1)	12.03 (43)	–	14.43 (1)	–
MILLWD	28.71 (43)	–	-9.72 (118)	–	8.19 (6)	–
NORTH	28.44 (2)	27.61 (1)	3.36 (18)	–	4.24 (4)	–
NYC	27.93 (66)	–	-3.08 (252)	–	7.76 (8)	–
WEST	15.06 (81)	21.58 (1)	7.63 (208)	–	9.85 (17)	–

31

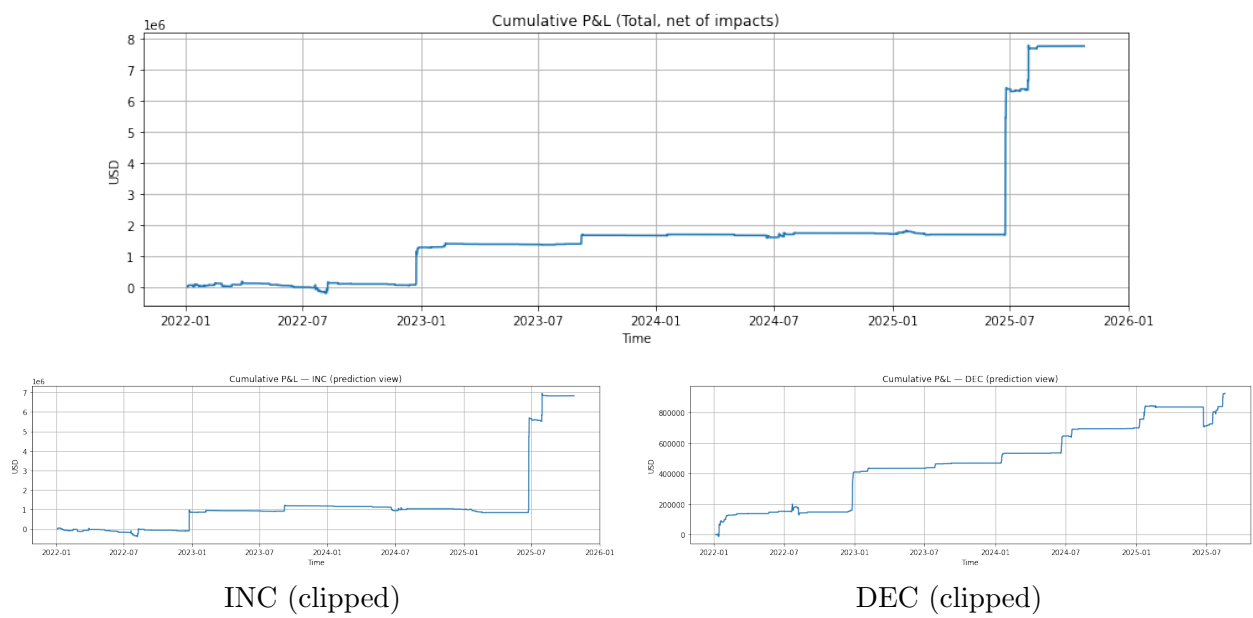INC (clipped)   DEC (clipped)

Figure 13: Cumulative P&L with side-frozen (clipped) strategy. Top: total portfolio; bottom: INC and DEC contributions.